Hindawi
Advances in Civil Engineering
Volume 2023, Article ID 8021378, 15 pages
https://doi.org/10.1155/2023/8021378

Research Article

Development of Fragility Curves for Reinforced-Concrete Building with Masonry Infilled Wall under Tsunami

Suthiwat Waenpracha,[1] Piyawat Foytong,[1] Anawat Suppasri,[2] Supakorn Tirapat,[1] Nuttawut Thanasisathit,[3] Pongnathee Maneekul,[4] and Teraphan Ornthammarath[5]

[1]*Sustainable Infrastructure Research and Development Center, Department of Civil Engineering, Faculty of Engineering, Khon Kaen University, Khon Kaen 40002, Thailand*
[2]*International Research Institute of Disaster Science, Tohoku University, Aoba, Sendai 980-8579, Japan*
[3]*Department of Civil Engineering, King Mongkut's University of Technology North Bangkok, Bangkok 10140, Thailand*
[4]*Division of Civil Engineering, Faculty of Engineering, Nakhon Phanom University, Nakhon Phanom 48000, Thailand*
[5]*Department of Civil and Environmental Engineering, Faculty of Engineering, Mahidol University, Nakhon Pathom, Nakhon Pathom 73170, Thailand*

Correspondence should be addressed to Piyawat Foytong; piyafo@kku.ac.th

Received 3 September 2022; Revised 22 February 2023; Accepted 4 March 2023; Published 14 March 2023

Academic Editor: Krishanu Roy

A tsunami is a natural disaster that destroys structures and kills many lives in many countries in the world. A risk assessment of the building under a tsunami loading is thus essential to evaluate the damage and minimize potential loss. A crucial tool in risk assessment is the fragility curve. Most building fragility curves for tsunami force were developed using survey building damaged data. This research proposed a method for developing fragility curves under tsunami loading based on the analytical building model data. In the development, the generic building was a one-story reinforced-concrete building with masonry-infilled walls constructed from the structural index, popularly built as residential buildings along the west coast of southern Thailand. Three damage levels were investigated: damage in masonry infill walls, damage in primary structures, and collapses. The masonry infill wall was modeled using multisprings to represent the load-bearing behavior due to tsunami with a hydrodynamic pattern. The fragility curves were developed using the maximum likelihood method and considering the uncertainty due to masonry infill wall type, tsunami flow direction, and tsunami flow velocity. The developed fragility curve agrees well with the empirical tsunami fragility curve of a one-story reinforced-concrete building damage data in Thailand from the 2004 Tsunami. The developed fragility functions could be adopted for assessing tsunami risk assessment and disaster mitigation for similar structures against different tsunami scenarios in the future.

1. Introduction

In the past, numerous natural disasters have killed individuals and severely damaged buildings. One natural disaster that significantly damages lives and property is the tsunami. There have been tsunami incidents that have seriously harmed. The Sumatra Tsunami on 26th December 2004 triggered a 9.1-magnitude earthquake in northern Sumatra and a tsunami in the Indian Ocean, which damaged more than 153,704 houses [1] along the coast of many countries and killed 227,898 people [2]. Samoa Tsunami on 29th September 2009, an 8.0-magnitude earthquake struck the Samoa Islands. It caused a tsunami to hit the Samoan archipelago and northern Tonga, damaging 326 homes [3] and killing 192 people [4]. On 11th March 2011, a 9.0-magnitude earthquake struck off the coast of Tohoku. It caused a tsunami and damaged more than 1,208,474 buildings; 15,899 people died, and 6,242 went missing [5], making it the most enormous tsunami in Japanese history. Risk assessment of buildings under a tsunami disaster is

needed to mitigate and prevent future damage. The key elements in risk assessment are the tsunami hazard map, building inventory, and tsunami fragility curve [6]. The tsunami hazard map is the data obtained from surveys or numerical simulations of a tsunami. The buildings inventory is the information obtained from the survey of buildings and structures in the risk area. Also, the tsunami fragility curve of the building structure can be generated from survey data of buildings and structures from each tsunami disaster and the analytical data from the montecarlo simulation method. Most fragility curves are represented as a function of tsunami inundation depth and are commonly generated by the least square and the maximum likelihood methods. In past research, the fragility curves were developed from historical events. Koshimura et al. [7] developed a fragility curve using numerical modeling of tsunami inundation and geographic data analysis (GIS) after the tsunami disaster at Sumatra Andaman in 2004. Suppasri et al. [8] developed a fragility curve of reinforced-concrete buildings and wooden buildings using data from satellite imagery to classify the damage and a numerical model of the 2004 Indian Ocean tsunami flooding in Thailand. Suppasri et al. [9] created a fragility curve from the Great Tsunami in Japan in 2011 of reinforced-concrete buildings, wooden buildings, and lightweight structures by considering the importance of the damage levels, the number of floors, and the location of the building. Gokon et al. [3] developed a fragility curve of wooden and reinforced-concrete structures of the 2009 Samoa earthquake and tsunami using a numerical model of the occurrence and spread of a tsunami. The building damage was monitored by visually interpreting changes with high-resolution satellite imagery before and after the tsunami. Nanayakkara and Dias [10] compared the fragility curves of researchers from different events to determine their similarity by comparing fragility curves according to the same building structure. Foytong and Ruangrassamee [11] developed an empirical tsunami fragility curve for one-story reinforced-concrete buildings and building taller than one-story reinforced-concrete buildings using tsunami-damaged data in the Indian Ocean in 2004 in Thailand. Aránguiz et al. [12] created a fragility curve of the masonry-wood composite structure using data from field surveys from the 2015 tsunami in Coquimbo, Chile.

This research studied the behavior and the fragility curve of the reinforced-concrete building model under tsunami in different flow directions. The analyzed reinforced-concrete building was a one-story building with masonry-infilled walls, a popular residential building constructed along the west coast of Thailand. The tsunami load was considered as a hydrodynamic force pattern distributed laterally throughout the inundation depth. Building models were analyzed by nonlinear pushover analysis using a plastic hinge to assess resistance following ASCE41-13 [13]. The masonry infilled walls would be simulated using multispring support, which was more suitable for analyzing under tsunami loading. The fragility curve was developed under the function of tsunami inundation height by considering the effect of turbulence from flow direction and velocity of the tsunami and the type of masonry infilled wall. Three damage levels in masonry infill walls, primary structures, and collapses were investigated. The analytical tsunami fragility curves were generated with the maximum likelihood method, which was suitable for building structural damage [14]. Finally, the fragility curve developed with the analytical approach was compared with the fragility curve of the one-story reinforced-concrete building generated from the 2004 tsunami damage survey data in Thailand [11].

2. Tsunami Damage

The two great tsunamis, the 2004 Indian Ocean tsunami and the 2011 Japan tsunami caused devastating damage to residential and public buildings. Large numbers of research on building damage characteristics due to tsunamis have started since then. Indonesia [7], Thailand [8], and Sri Lanka [15] were the main countries where tsunami fragility functions were developed using damaged building data from the 2004 tsunami. Previous studies in the Indian Ocean region show that most buildings were totally damaged when the tsunami flow depth was larger than 2 m. Suppasri et al. [16] assessed the RC building column performance based on a full-scale pushover experiment of the column and the whole building frame. Although the fragility functions were developed and showed some differences among each country, these empirical functions were developed using limited samples. On the other hand, damaged building data were perfectly collected in the case of the 2011 Japan tsunami. About 250,000 damaged buildings around the East Japan region were used to develop various kinds of tsunami fragility functions [17]. They found that most Japanese buildings were totally damaged when the flow depth was higher than 3 m [9] and the damage characteristics also obviously depended on flow velocity as a result of the coastal topography [18]. Figure 1(a) shows an example of damage to a typical residential house in Ishinomaki City. The house was flooded by about 4 m inundation depth, but the damage only occurred mainly at nonstructural members, such as walls and less damage to structural members, such as the small column. In addition, an obvious issue on the overturned buildings (Figure 1(b)) also attracted interest from the structural design point of view as these buildings had no severe structural damage but failed because of piles and foundations due to liquefaction as a result of the earthquake [19]. Similar to the case of the 2004 tsunami, the fragility functions were developed using empirical relationships from large numbers of data on the macro scale. Nevertheless, such analytical and experimental microscale studies are also necessary.

3. Generic Building

The analyzed buildings used in this study was representative reinforced-concrete building generated from the average structural index of the residential construction drawings along the west coast of Thailand [20]. The building was 9 meters wide, 10 meters long, and 3 meters high. The

(a) (b)

Figure 1: Damage of building. (a) An example of damage to a typical residential house in Japan. (b) An example of overturned building in Onagawa town. The building had fewer openings and failure of the pile foundation was observed.

ground plan and roof plan are shown in Figure 2. There were nine columns with 20 cm × 20 cm cross-sections. The longitudinal reinforcement was 4-DB12 mm, and the stirrups were RB6@150 mm. The roof beam section was 20 cm × 40 cm with the longitudinal reinforcement of 5-DB16 mm and stirrups RB6@150 mm. The section detail of the column and beam section can be shown in Figure 3. The average tensile strengths of the reinforcement are listed in Table 1. The compressive strength of concrete was 23.5 MPa. Three types of masonry-infilled walls in the building, WallA, WallB, and WallC, are shown in Figure 4. WallA is located on the front and back of the building with an opening area of 25.0 percent. The opening area of WallB is 7.5 percent, situated on both sides of the building. And, WallC is on the front, back, and middle of the building with an opening area of 28.5 percent.

4. Tsunami Force

According to previous research and standard codes, tsunami forces on building structures can be considered in the form of forces such as hydrostatic forces, buoyant forces, hydrodynamic forces, impulsive forces, debris impact forces, debris damming forces, uplift forces, and additional gravity loads from retained water on elevated floors. However, hydrodynamic force is the most suitable force pattern in the analysis of forces acting on buildings due to tsunamis [21–25]. A hydrodynamic force pattern is a lateral force that is uniformly distributed throughout the depth, which was determined using the equation proposed by FEMA 55 [21] as equation (1), where ρ is the water density, C_D is the drag coefficient, b is the width of the building, h is the flow depth, and V is the flow velocity. It can be seen that the force acting depends on the depth and flow velocity of the tsunami. Therefore, in the analysis of building models, static pushover analysis was performed by stabilizing the inundation depth and increasing the force by increasing the flow velocity until the building collapsed. The inundation depth was considered from 0.5 m to 3 m with increments of 0.25 m.

$$F_d = \frac{1}{2}\rho C_D b h V^2. \quad (1)$$

5. Building Model

The building model was analyzed using a 3-dimensional nonlinear static pushover analysis method to study the behavior of reinforced-concrete structures with masonry-infilled walls under a tsunami loading. The building model consisted of the bare frame and masonry-infilled wall models. Details are as follows.

5.1. Bare Frame Model. The bare frame model consisted of elastic elements and plastic hinges located at the end of beams and columns to represent their nonlinear behavior, as shown in Figure 5. The plastic hinge lengths were calculated using the equation proposed by Paulay and Priestley [26], as shown in equation (2), where L was the distance from a critical section to the point of contraflexure, d_b was the diameter of longitudinal reinforcement, and f_y was the yield stress of longitudinal reinforcement. The plastic hinge of the columns, 4.5 m beams, and 5.0 m beams are 0.34 m, 0.55 m, and 0.59 m, respectively. The behavior of plastic hinges was defined by ASCE 41-13 [13]. The beam and column joints were connected with a rigid member. The building model used fixed support. In addition, the shear capacity of columns and beams was analyzed using the equation proposed by Sezen [27] by considering the axial force of each column from the vertical load. The axial force, shear strength, and flexural strength of each column and beam can be shown in Table 2.

$$L_p = 0.08L + 0.022 d_b f_y. \quad (2)$$

5.2. Masonry-Infilled Wall Model. Using a single spring model diagonal from one top corner to one bottom corner, as analyzed the model under seismic load, was not appropriate to assess the model behavior under tsunami load. The simulated tsunami force was uniformly in the hydrodynamic forces pattern through the inundation depth. Therefore, the masonry-infilled wall behavior is modeled with multisprings distributed according to the bare frame height, as shown in Figure 6. The tsunami load was transferred from the impacted side column to the column on the other side through

Table 1: Properties of reinforcement.

Diameter (mm)	Yield strength (MPa)	Yield strain	Elastic modulus (GPa)
6	319	0.00365	224
12	451	0.00240	203
16	549	0.00330	209

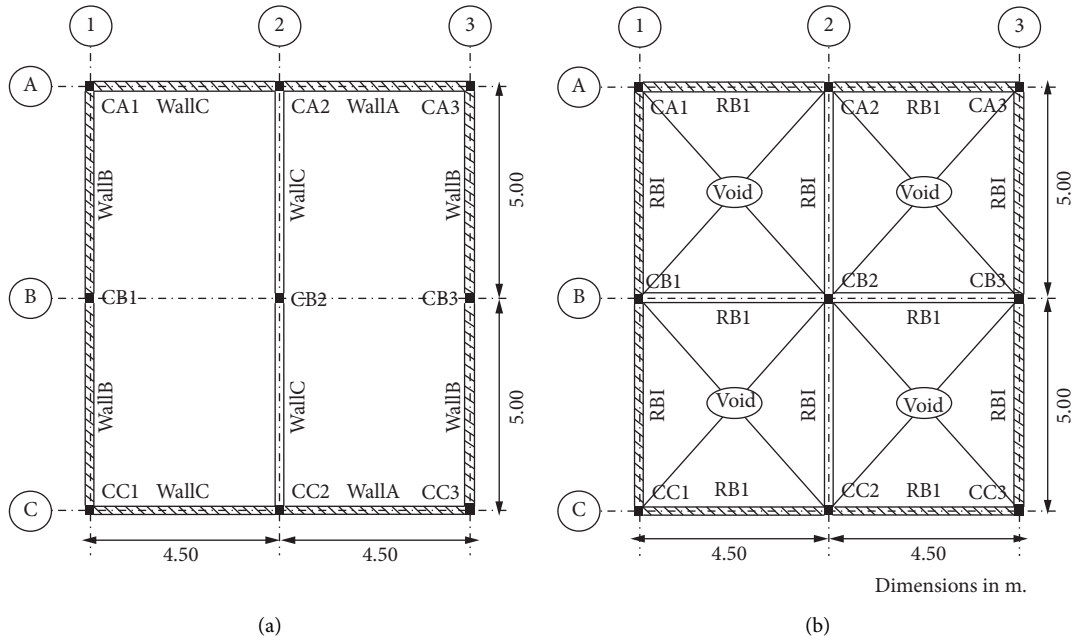

Figure 2: Construction drawing of the building. (a) Floor plan. (b) Roof plan.

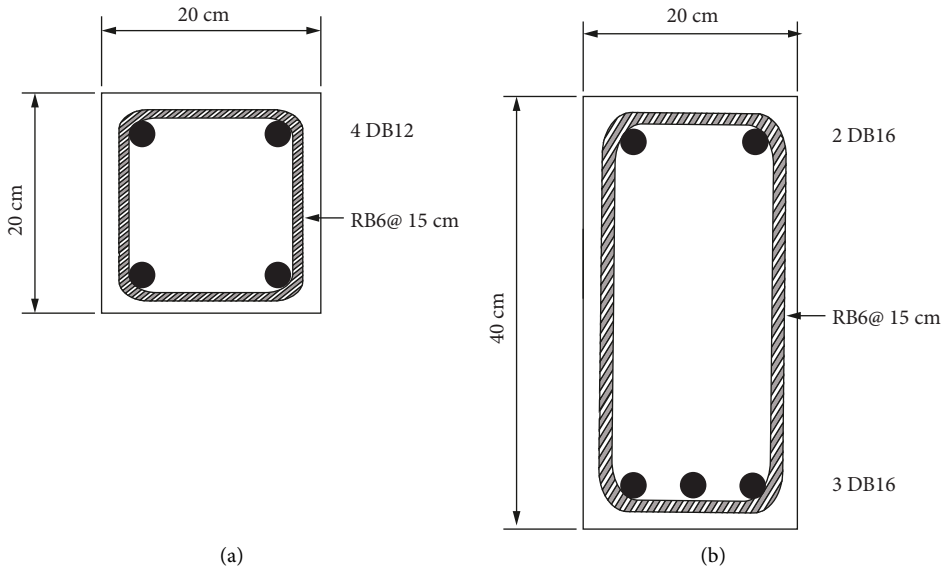

Figure 3: The section detail of column and beam. (a) Column section. (b) Beam section.

axial springs and rigid links [28]. The plastic hinges across the column height at the top and bottom of each spring to capture the nonlinear behavior of columns at concentrated force joints. The lateral load resistance for the wall with openings decreased by the amount of opening area on the wall panel.

The building model was analyzed with three types of masonry infilled walls and considered two types of masonry,

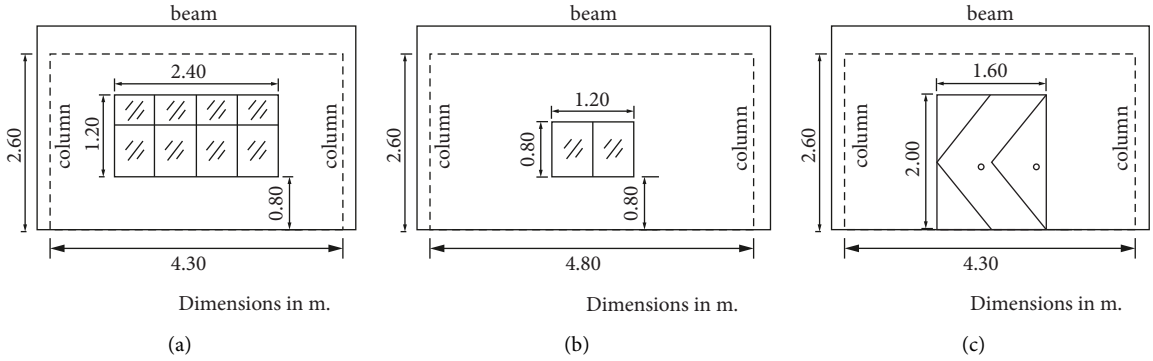

Figure 4: Configurations and dimensions of the masonry-infilled walls. (a) WallA. (b) WallB. (c) WallC.

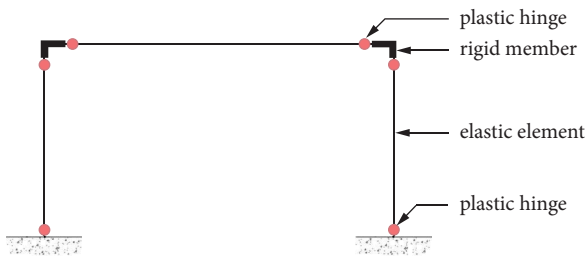

Figure 5: Bare frame model.

Table 2: Axial force, shear strength, and bending moment of columns and beams.

Location	Axial force (kN)	Shear capacity (kN)	Bending moment capacity (kN-m)	Cracking moment capacity (kN-m)
CA1, CA3, CC1, CC3	7.99	41.70	19.24	4.05
CA2, CC2	8.26	41.72	19.26	4.05
CB1, CB3	15.99	42.45	19.91	4.05
CB2	16.51	42.50	19.95	4.05
RB1	—	60.31	127.79	—

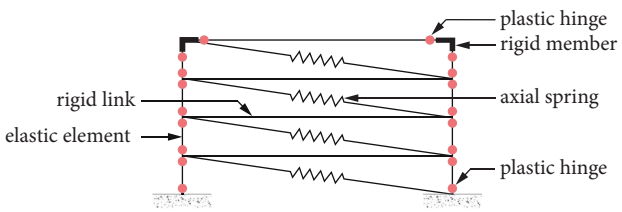

Figure 6: Model of multispring masonry infilled wall.

hollow brick (HB) and clay brick (CB), which were the most commonly used in Thailand. The compressive strength HB and CB according to ASTM C1314-03b [29] were 3.81 MPa and 4.12 MPa at the corresponding strain of 0.0049 and 0.0071, respectively, [30]. The masonry infilled wall behavior was modeled with the relationship between lateral load resistance and displacement, consisting of 3 parts: yield point (y), maximum resistance (m), and residual resistance (p). The controlled parameters, resistance, and deformation, are shown in Table 3. The clay brick wall (CW) could resist lateral loads more than the hollow brick wall (HW) for the same masonry-infilled wall type. The lateral resistance of walls depended on the opening percentage, which can be arranged as WallB, WallC, and WallA, respectively.

The out-of-plane resistance of the masonry infilled wall under the lateral load is highly less than the in-plane resistance. However, when subjected to out-of-plane force, the masonry-infilled wall behavior was considered to determine the damage level occurring in masonry-infilled walls in the process of creating fragility curves. The masonry-infilled wall out-of-plane behavior was calculated in the equation proposed by FEMA 306 [31]. The masonry-infilled wall of the building model had an out-of-plane force resistance for HW and CW of 0.00022 MPa and 0.00063 MPa, respectively.

6. Analysis and Behavior of Buildings under Tsunami Loading

6.1. Building Analysis. In the one-story reinforced-concrete building with masonry infilled-wall analysis, the static pushover analysis was applied to simulate the tsunami forces acting on the building in the hydrodynamic force pattern, a uniformly distributed lateral force throughout the inundation depth. The tsunami load acting on the building was

Table 3: Lateral resistance and deformation of masonry-infilled walls.

Type of wall	Type of brick	V_y (kN)	V_m (kN)	V_p (kN)	U_y (m)	U_m (m)	U_p (m)
WallA	HB	30.29	40.39	12.12	0.00898	0.02395	0.02450
	CB	111.87	149.16	44.75	0.01298	0.03461	0.03500
WallB	HB	35.68	57.57	14.27	0.00808	0.02155	0.02200
	CB	137.95	183.94	55.18	0.01168	0.03114	0.03150
WallC	HB	31.35	41.80	12.54	0.00898	0.02395	0.02450
	CB	119.74	159.65	47.90	0.01298	0.03461	0.03500

modeled by fixing the inundation depth to obtain a load pattern and increasing the magnitude of the force by increasing the tsunami flow velocity until the building model collapsed. The tsunami inundation depths were considered from 0.5 m to 3 m with an incremental of 0.25 m equally. Four directions of water impact on the building were considered: the flow direction of 0°, 30°, 60°, and 90°, as shown in Figure 7. The masonry-infilled walls encountered water were disappeared due to less resistance of the out-of-plane failure. Therefore, in the cases of the flow direction of 30° and 60°, there is no masonry-infilled wall in the analysis model. The applied tsunami forces acting on columns of all flow direction cases are shown in Figure 8.

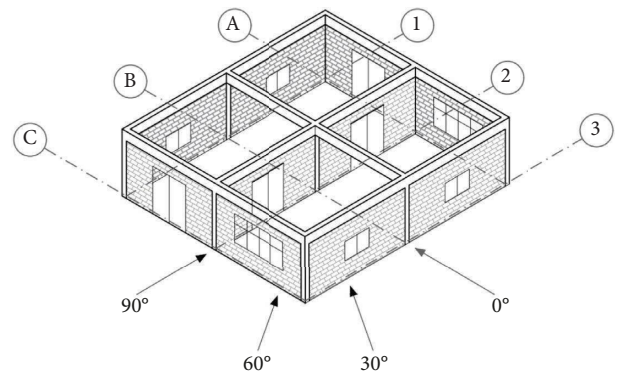

Figure 7: Tsunami flow direction.

6.2. Building Behavior under Tsunami Force. The lateral resistance and roof deformation relationships of a generic one-story reinforced-concrete building with two types of masonry-infilled wall model under tsunami flow directions of all flow direction cases are shown in Figures 9 and 10. The failure modes and failure members of all flow direction cases are shown in Table 4. For all inundation depths, the masonry-infilled walls were subjected to water encountered due to rapid out-of-plane failure. The buildings analyzed in the 0° flow direction would have no masonry-infilled walls built-in gridlines 1, 2, and 3. The buildings analyzed in the 30° and 60° flow directions would have no masonry-infilled walls built-in all gridlines. There are no masonry-infilled walls built-in gridlines A and C for the buildings analyzed in a 90° flow direction. The damage to structural components would be caused by the moment cracking of concrete in the columns. The damage would begin at an inundation depth of 0.75 m in the flow direction of 0°, 30°, and 60°. At low inundation depths, buildings were prone to damage as low inundation depths make columns challenging to bend, resulting in high lateral resistance during damage. Furthermore, as the inundation depths in the analysis increased, the lateral resistance of the building during damage would gradually decrease, as shown in Figures 9(a)–9(f). The flow direction of 90° differed from other flow directions because, in this flow direction, there is a masonry-infilled wall to support the load. In low inundation depths, most load-bearing masonry-infilled walls will support sections at the same level as the inundation depth. The higher the inundation depth, the more support the masonry-infilled wall will be able to bear more force so that at low inundation depths, the building will be more prone to damage during higher inundation depths, as shown in Figures 10(a) and 10(b). The analysis also found that when the column reached the yield point, it would result in the building model stiffness value being clearly reduced, and when the wall had the strength in the plane to the yield point, it would result in a decrease in the stiffness of the building as well.

6.2.1. Buildings under Tsunami in the 0-Degree Flow Direction. From the analysis of the buildings in the 0° direction, as shown in Figures 9(a) and 9(b), it was found that the CW buildings had slightly increased lateral resistances from 220.81 kN to 225.42 kN over an inundation depth of 0.50 m to 1.25 m. The model was controlled by the shear failure in Column B2, a column that did not connect to the masonry-infilled wall. For inundation depths of 1.50 m to 2.50 m, the building lateral resistance increased dramatically from 230.91 kN to 269.87 kN. As the inundation depth increased, the masonry-infilled wall could bear more strength in the area exposed to the inundation depth and the shear failure in Column B2 controlled the building. In the inundation depths of 2.75 m to 3.00 m, the building changed failure mode from a shear failure in column B2 to a flexural failure in column B2 with the lateral resistance of the building decreasing from 357.76 kN to 330.79 kN. In the analysis of HW buildings, it was found that the building behavior of all inundation depths was the same as that of the CW buildings but had less side resistance than the CW buildings.

6.2.2. Buildings under Tsunami in the 30-Degree Flow Direction. Flow direction analysis of the building in the 30° direction revealed that the building had a slight decrease in its lateral resistance from 433.23 kN to 428.78 kN over an inundation depth of 0.50 m to 2.00 m. The building model

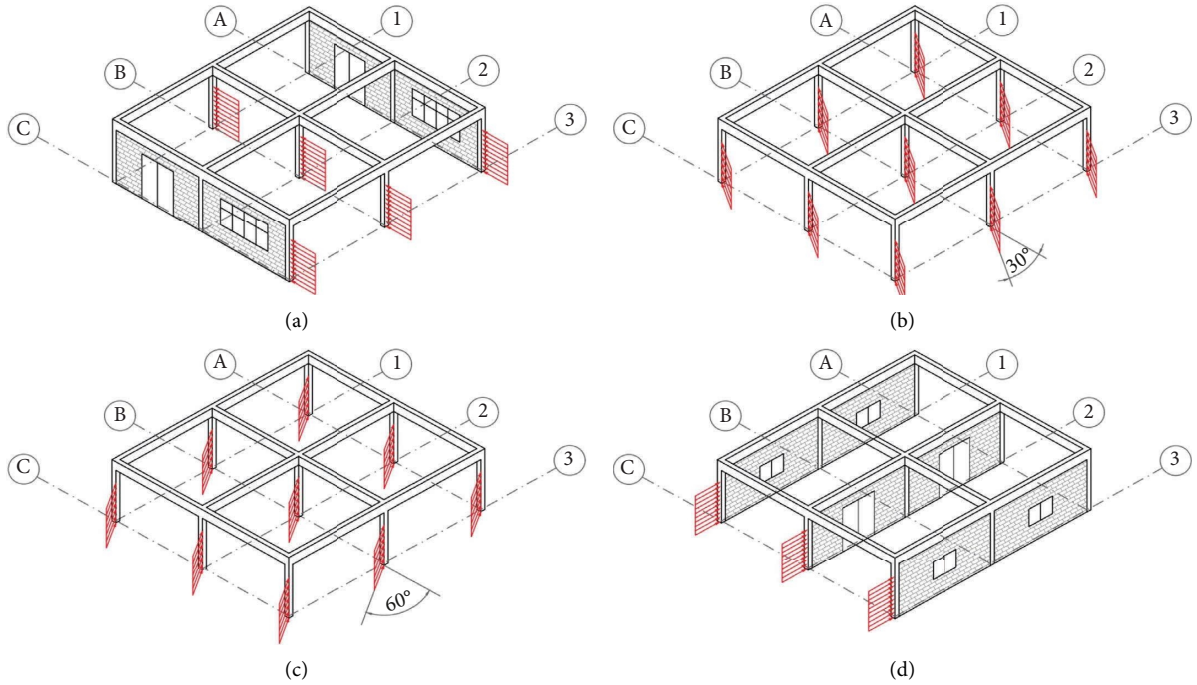

Figure 8: Applied tsunami forces acting on the building columns in each flow direction. (a) 0°. (b) 30°. (c) 60°. (d) 90°.

was controlled by the shear failure in Columns A2 and C2 because the building had no masonry-infilled walls and water had acted on every column of the building simultaneously. There was a dividing force between the columns in each bare frame, thus causing a collapse at the central column of each bare frame. In the inundation depths of 2.25 m to 2.50 m, the building changed from a shear failure in columns A2 and C2 to a flexural failure in columns A2 and C2, with the lateral resistance reduced from 412.15 kN to 366.03 kN. And, for inundation depths of 2.75 m to 3.00 m, the high inundation depth up to the beam caused the columns in gridline B to bear more load from the beams than the other columns. As a result, the building was controlled by flexural failure in column B2 with the building lateral resistance reduced from 234.55 kN to 203.23 kN, as shown in Figures 9(c) and 9(d).

6.2.3. Buildings under Tsunami in the 60-Degree Flow Direction. For the analysis of buildings in the 60° direction, as shown in Figures 9(e) and 9(f), it was found that the failure behavior at all inundation depths was similar to the 30° flow direction. The lateral resistance of the CW building slightly decreased from 440.72 kN to 432.94 kN in the inundation depth range of 0.50 m to 2.00 m. The shear failure in Columns B1 and B3 controlled the building. In the inundation depth of 2.25 m to 2.50 m, the failure mode was changed from a shear failure in columns B1 and B3 to a flexural failure in columns B1 and B3, with the building lateral resistance reducing from 411.57 kN to 365.13 kN. And, for inundation depths of 2.75 m to 3.00 m, a flexural failure occurred in column B2, with the building lateral resistance reduced from 239.07 kN to 205.98 kN.

6.2.4. Buildings under Tsunami in the 90-Degree Flow Direction. For the analysis of buildings in the direction of 90°, as shown in Figures 10(a) and 10(b), when the inundation depth was increased, the CW building had a significant increase in lateral resistance, resulting in more loading at the masonry-infilled wall. The lateral resistance increased from 162.22 kN to 514.65 kN over an inundation depth of 0.50 m to 2.50 m. The building failure was controlled by the shear failure in Columns A1, A2, and A3. For inundation depths of 2.75 m to 3.00 m, which was the high inundation depth up to the beams caused the columns in Gridline 2 to bear more load from the beams than the others, causing the building to have flexural failures in columns A2 and C2, with the lateral resistance reducing from 993.67 kN to 889.45 kN.

7. Development of Fragility Curve

This research developed the analytical tsunami fragility curves for a generic one-story reinforced-concrete building with masonry-infilled walls. The main components included the determination of the degree of damage, variables with uncertainty, and parameter estimation of the fragility curve by the maximum likelihood method, with details as follows.

7.1. Damage Level. Analysis of the building model revealed that the model was damaged in both the secondary and primary members. Therefore, damage levels were divided into three levels described as follows:

(1) Damage in secondary members (damage level 1, DL1): the masonry-infilled wall broke off by an

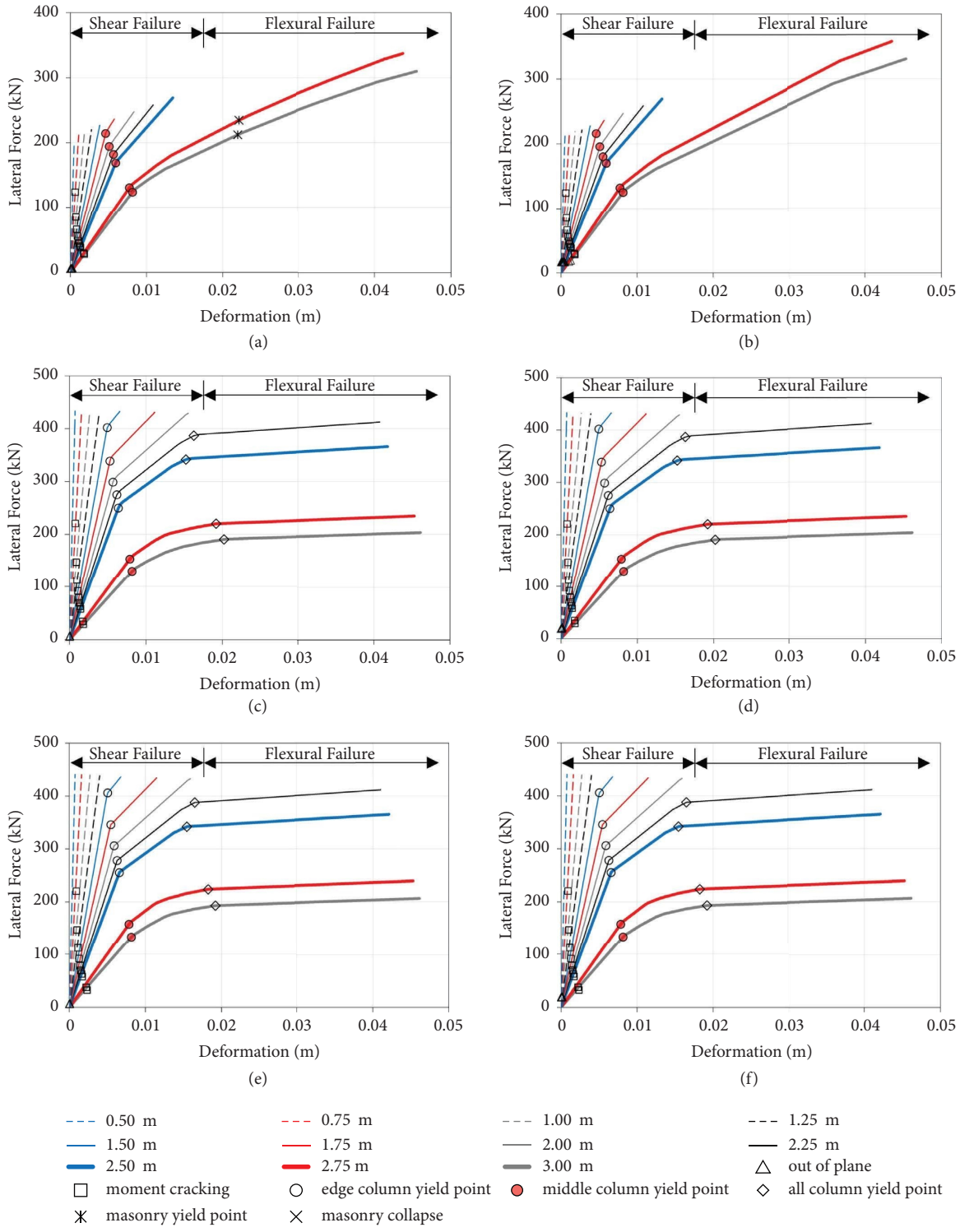

Figure 9: Relationship of lateral resistance and roof deformation of hollow brick walls (HB) and clay brick walls (CB) for 0°, 30°, and 60° flow directions. (a) HB-0°. (b) CB-0°. (c) HB-30°. (d) CB-30°. (e) HB-60°. (f) CB-60°.

out-of-plane force or reached the yield point of the in-plane capacity

(2) Damage in primary members (damage level 2, DL2): beams or columns were cracked, which is the beams or columns reached their cracking moment capacity, but the building model was still sustained

(3) Collapse (damage level 3, DL3): the building model was subjected to shear or flexural failure at columns, and the building model was terminated

7.2. Uncertainty Variables. In order to construct the fragility curves from the model analysis data, it is necessary to take into account the potential uncertainties in two parts: the resistance of the building model and forces affecting model damage behavior under tsunami force. In this research, three uncertainty variables were identified: (1) the type of brick used as a building masonry infilled wall, which was the uncertainty variable in the resistivity of the model; (2) tsunami flow velocity was an uncertain variable of tsunami behavior; and (3) tsunami flow direction was uncertainty variable in the direction action force.

7.2.1. Brick Type of Masonry Infilled Wall. Hallow brick and clay brick are commonly used as walls in reinforced-concrete residential buildings in Thailand. Two types of bricks have different lateral load resistances that affect the behavior of the building model under tsunami forces. The uncertainty of these two types of masonry will be taken into account in equal ratios.

7.2.2. Tsunami Flow Velocity. Tsunami flow velocity is a very high uncertainty value independent of inundation depth. In addition, the tsunami flow velocity is an essential parameter in estimating the force exerted by a tsunami on a building structure. Many past studies have attempted to estimate the velocity of tsunamis both theoretically and observed after tsunami events [21, 32–34]. Nevertheless, it cannot clearly determine the tsunami flow velocity. It can only be defined as a function of the tsunami inundation depth that is in the range of $0.7\sqrt{gh}$ to $2.0\sqrt{gh}$. Therefore, in this research, the flow velocity range was determined to be used to consider the data. In the fragility curve development, the maximum likelihood estimators are calculated based on the amount of damage data incurred for each considered damage level by selecting only damage data within the tsunami flow velocity range. Damage data with flow velocities greater than the upper boundary range will not be considered. Moreover, the damage data with flow velocity below the lower boundary range is absolute damage; therefore, it cannot be taken for probabilistic calculations.

7.2.3. The Direction of the Tsunami Flow. The tsunami flow direction is one of the uncertainty variables that can occur, which was taken into account in the amount of damage data for the flow direction of 0°, 30°, 60°, 90°, 120°, 150°, and 180°. The data for the flow direction of 120°, 150°, and 180° were used for the directions of 60°, 30°, and 0°, respectively. In this study, the distribution of damage data in each flow direction was determined according to the normal distribution characteristics, as shown in Figure 11, in order to conform to the actual building site location of the buildings, in which most were facing the beach. Therefore, the direction at 90° in front of the building had been determined to have the greatest amount of data due to the high probability of a tsunami hitting it. The direction at 0° and 180°, the side directions of the building, were determined to have the least amount of data due to the low probability of a tsunami hitting them.

The relationships of tsunami flow velocity at each damage level and inundation depth with the variety of the tsunami flow direction within the tsunami flow velocity boundary are shown in Figure 12. The analysis revealed that at damage level 1, damage in masonry infilled wall, only CW buildings were damaged during the tsunami flow velocity range at an inundation depth of 0.50 m, as shown in Figure 12(b). For damage level 2, damage in structural members, both brick wall buildings were damaged in the tsunami flow velocity range at inundation depths of 1.50 m to 2.50 m for a flow direction of 0°, at inundation depths of 1.25 m to 2.50 m for a flow direction of 30° and 60° and at an inundation depth of 2.75 meters for 90° flow directions as shown in Figures 12(c) and 12(d). Furthermore, for damage level 3, building collapse, both brick-walled buildings would collapse in the tsunami flow velocity range at 2.75 meters to 3.00 meters of inundation depth for 0° flow direction, at 2.50 meters to 2.75 meters of inundation depth for 30° and 60° flow direction. For the flow direction of 90°, as shown in Figures 12(e) and 12(f), the CW buildings would be collapsed in the boundary of the tsunami flow velocity at an inundation depth of 3.00 meters, and the hallow brick wall buildings would be collapsed at inundation depths of 2.75 m to 3.00 m.

Considering the damage data under the uncertainty variables, brick wall types, the tsunami flow velocity, and the tsunami flow directions, the number of damage data for levels 1, 2, and 3 using the Montecarlo Simulation method were 69, 446, and 238, respectively. The number of damage data for all three damage levels in each inundation depth used to develop fragility curves is shown in Table 5.

8. Fragility Curves Using the Maximum Likelihood Method

In this study, fragility curves for each damage level were developed using data from the building analysis data of two masonry-infilled wall building models with the uncertainty variables as a function of the inundation depth for each damage level. The development of the fragility curve took the form of a lognormal distribution function of two parameters, which consists of the median and the lognormal standard deviation. The maximum likelihood method would be used to estimate the two parameters, as shown in equation (3), and the fragile curve can be written as a lognormal function, as in equation (4).

$$M\prod_{k=1}^{N_h}\left[F\left(a_{N_h}\right)\right]^{P_{N_h,k}}\left[1-F\left(a_{N_h}\right)\right]^{1-P_{N_h,k}}, \tag{3}$$

$$F(a)=\Phi\left[\frac{\ln\left(a/\alpha\right)}{\beta}\right], \tag{4}$$

where a_{N_h} = the k-th inundation depth. $P_{N_h,k}$ = the cumulative probability of building damage of the k-th Inundation Depth. $\Phi(.)$ = the standardized normal distribution function. N_h = the total number of considered inundation depths. α, β = median and lognormal standard deviation of inundation depth in a unit of meter.

Table 4: Failure mode and failure members of all flow direction cases.

Inundation depth (m)	Failure mode and failure members							
	0°		30°		60°		90°	
	Failure mode	Member	Failure mode	Member	Failure mode	Member	Failure mode	Member
0.50								
0.75								
1.00								
1.25			Shear	CA2 CC2	Shear	CB1 CB3	Shear	CA1 CA2 CA3
1.50	Shear	CB2						
1.75								
2.00								
2.25				CA2 CC2		CB1 CB3		
2.50			Flexure		Flexure			
2.75								CA2 CC2
3.00	Flexure	CB2		CB2		CB2	Flexure	

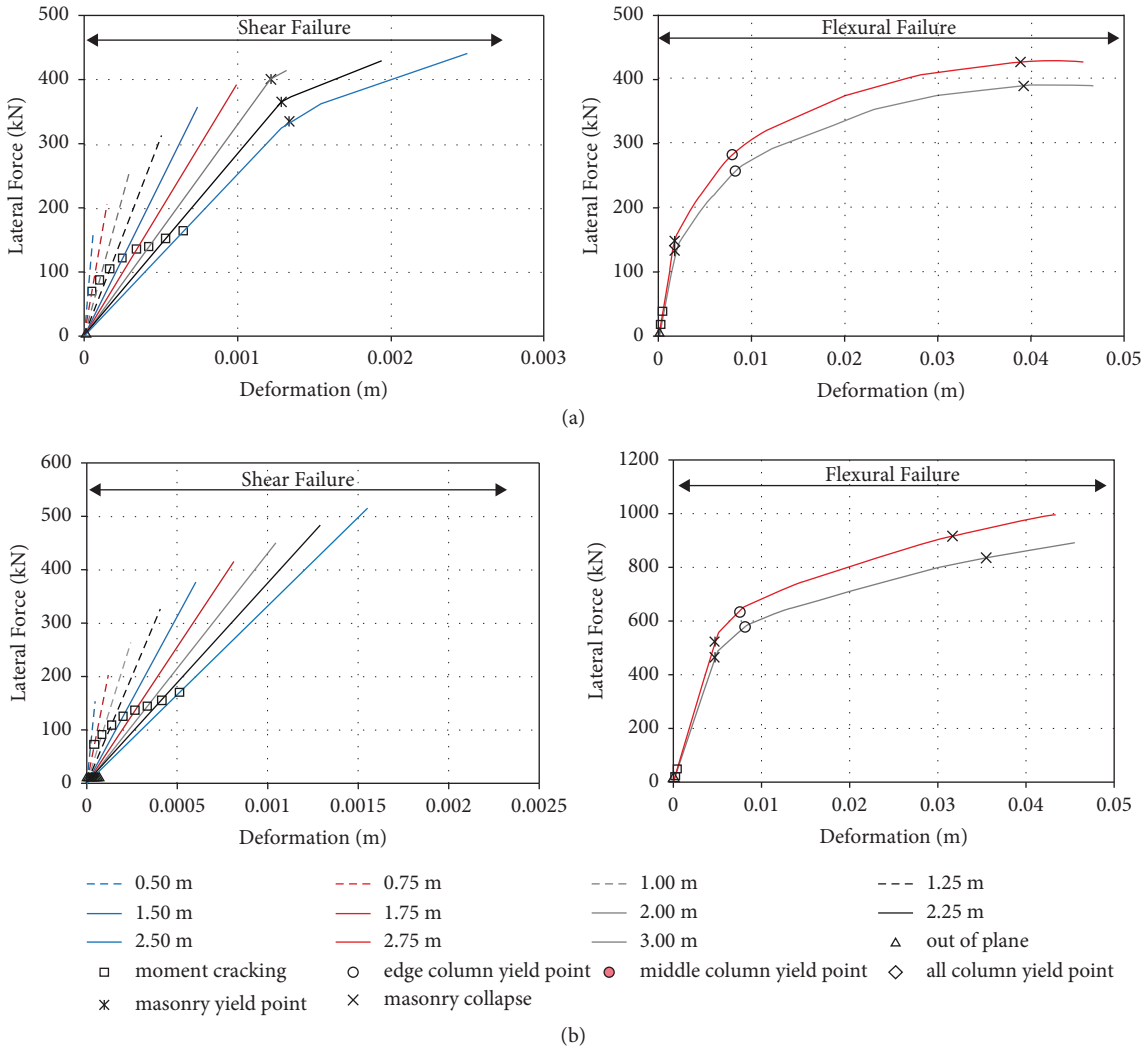

Figure 10: Relationship of lateral resistance and roof deformation of hollow brick walls (HB) and clay brick walls (CB) for 90° flow directions. (a) HB-90°. (b) CB-90°.

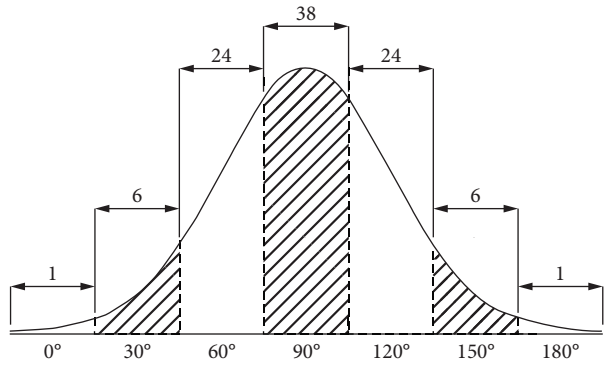

Figure 11: The distribution of the amount of damage data in each flow direction.

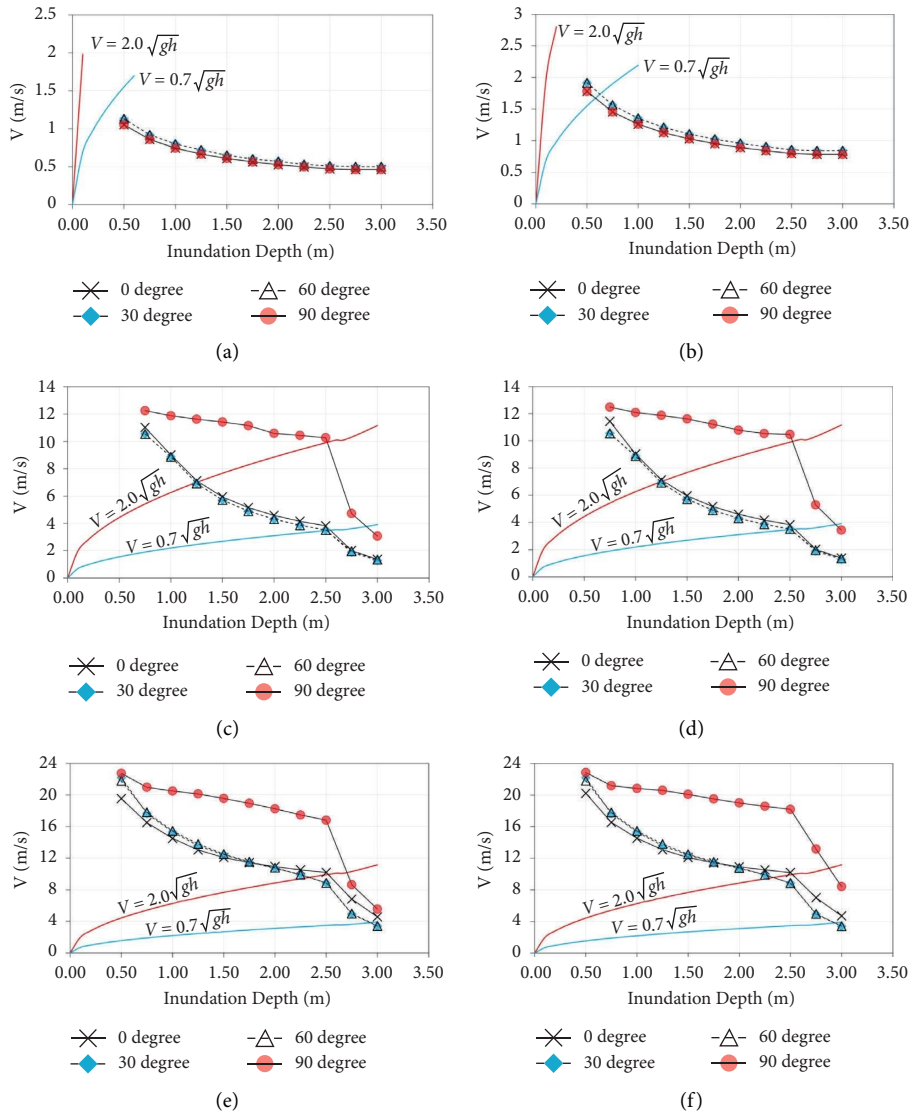

Figure 12: Damage data at each inundation depth within the tsunami flow velocity boundary. (a) DL1 with HW. (b) DL1 with CW. (c) DL2 with HW. (d) DL2 with CW. (e) DL3 with HW. (f) DL3 with CW.

Table 5: Number of damage data considered for uncertainty variables.

Flow direction	Damage level	Amount of damage data according to inundation depth (m)										
		0.50	0.75	1.00	1.25	1.50	1.75	2.00	2.25	2.50	2.75	3.00
0°	DL1	1	—	—	—	—	—	—	—	—	—	—
	DL2	—	—	—	—	2	2	2	2	2	—	—
	DL3	—	—	—	—	—	—	—	—	—	2	2
30°	DL1	6	—	—	—	—	—	—	—	—	—	—
	DL2	—	—	—	12	12	12	12	12	12	—	—
	DL3	—	—	—	—	—	—	—	—	12	12	—
60°	DL1	24	—	—	—	—	—	—	—	—	—	—
	DL2	—	—	—	48	48	48	48	48	48	—	—
	DL3	—	—	—	—	—	—	—	—	48	48	—
90°	DL1	38	—	—	—	—	—	—	—	—	—	—
	DL2	—	—	—	—	—	—	—	—	—	76	—
	DL3	—	—	—	—	—	—	—	—	—	38	76

Table 6: Parameters of fragility curves for each damage level.

Types of parameters	DL1		DL2		DL3	
	α	β	α	β	α	β
Not limited β	0.482	1.087	1.768	1.299	0.589	1.064
Limited β	0.482	1.087	1.788	1.219	2.620	1.219

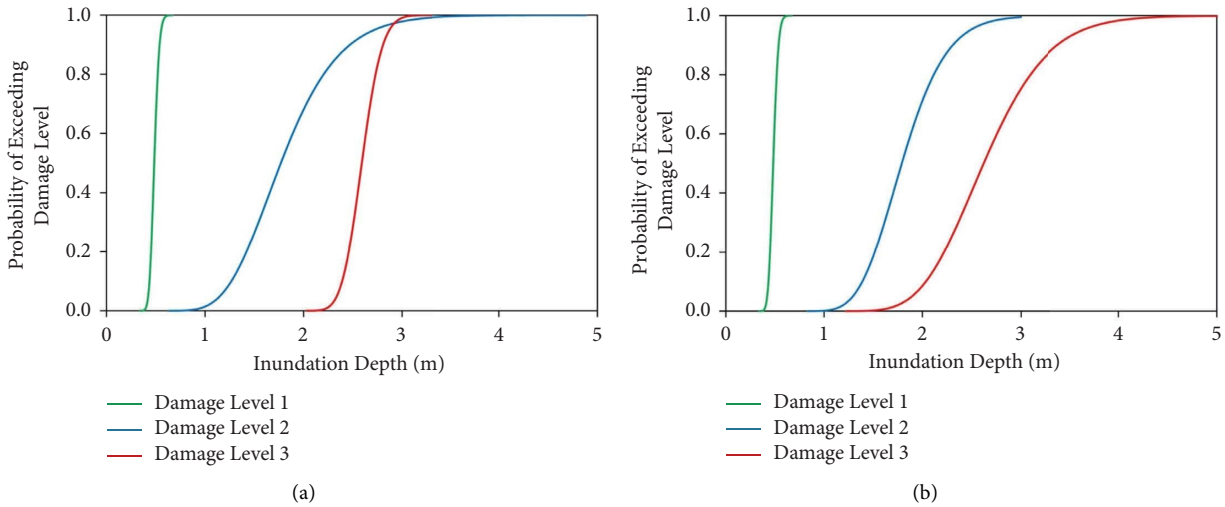

Figure 13: Analytical fragility curve of the building. (a) All damage levels without limiting the standard deviation. (b) All damage levels by limiting the standard deviation.

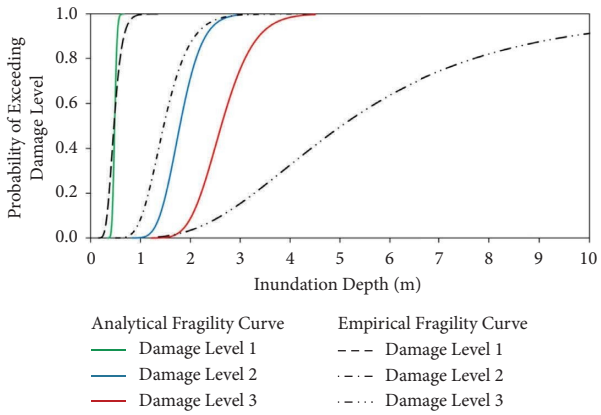

Figure 14: A comparison of the analytical fragility curve with the empirical fragility curve proposed by Foytong and Ruangrassamee [11].

The parameters α and β are calculated to determine the optimization to maximize $\ln(M)$ values by taking the derivative of $\ln(M)$ relative to α and β with values equal to zero as shown in the following equation:

$$\frac{d\ln(M)}{d\alpha} = \frac{d\ln(M)}{d\beta} = 0. \quad (5)$$

To calculate the parameters α and β of the fragility curves, the researcher began by substituting the cumulative probabilities of the damage data $(P_{N_h,k})$ and the inundation depth (a_{N_h}) in equation (4) to obtain the most suitable parameters, in which the fragility curve for each damage was plotted using the inundation depth (a_{N_h}) value and both parameters.

Damage data for all damage levels taken into account uncertainty variables were brought to create the fragility curves for each damage level. The tsunami fragility curve parameters are expressed in Table 6. The fragility curves for all damage levels are shown in Figure 13(a). It was found that at an inundation depth of water of 2.9 m, the fragility curve of damage level 2 overlapped damage level 3 because the amount of damage data of both levels were inversely proportional to the dispersion in each flow direction. The standard deviations for both damage levels will be equalized to avoid the intersection, according to the proposed by Shinozuka et al. [35]. The parameters of the limiting standard deviations for all damage levels as shown in Table 6. The fragility curves for all damage levels that are limited to standard deviations are shown in Figure 13(b). The damage level 1 has a probability of damage equal to 1 at an inundation depth of 0.75 m. At higher damage levels, the probability of damage was lower at the same water level, where the inundation depth of 3 m of damage level 2 and inundation depth of 4.5 m of damage level 3 was the inundation depth with a probability of damage of 1.

Figure 14 shows the comparison of the developed analytical fragility curves with the empirical fragility curves collected from one-story building damage data from past tsunami events in southern Thailand [11] of all damage levels. It was found that at damage level 1, the fragility curves were similar. In the beginning, the probabilities of empirical fragility curves were slightly higher than those of analytical fragility curves at the same inundation depth and intersection at 0.5 m inundation depth in which after the point of intersection, the analytical fragility curve has a higher probability than the

empirical fragility curve. For damage level 2, the empirical fragility curve had a higher probability value than the analytical one at the same inundation depth. For damage level 3, the analytical fragility curve was significantly higher than the empirical fragility curve at the same inundation depth.

9. Conclusions

This research analyzed the behavior and developed the fragility curve of the generic one-story reinforced-concrete building model, which is the typical residential construction along the west coast of Thailand. In this study, the static pushover analysis was adopted in order to model the effect of tsunami force on the selected structures. For uncertainties, different variables have been considered, including different brick types of masonry-infilled walls, tsunami flow velocities, and different tsunami flow directions. Some significant observations could be listed as follows:

(1) The analysis shows that out-of-plane damage in the masonry-infilled wall is the first damage state for all analysis cases since the inundation of 0.50 m because of less capacity. The future mechanisms are cracking and failure in columns. The lateral resistance of in-plane masonry-infilled walls is much higher than that of columns; therefore, the behaviors of a building model with clay brick walls were slightly higher than that with hollow brick walls; however, they were pretty much the same. The tsunami flow directions significantly affected the building model behavior because the flow direction is the specified parameter for the out-of-plane failure in the masonry-infilled wall. Considering the boundary of tsunami flow velocity, the failure modes of columns are a shear failure for low inundation depth and a flexural failure at the inundation depth of 1.25 m for 0°, 30°, and 60° tsunami flow directions and at the inundation depth of 2.50 m for 90° tsunami flow direction. The analyzed building model collapsed at the inundation depth of 2.50 m for 0°, 30°, and 60° tsunami flow directions and at the inundation depth of 3.00 m for 90° tsunami flow direction

(2) The three damage fragility curves were generated using the maximum likelihood method as a function of inundation depth using damage data from two brick wall models analyzed with the uncertainty variables of the brick wall, the distribution of the flow direction, and the tsunami flow velocity in the range of $0.7\sqrt{gh}$ to $2.0\sqrt{gh}$. The damage in the secondary members was occurred when the tsunami inundation depth was higher than 0.75 meters. At the tsunami inundation depth of about 1.80 meters, the probability of exceeding damage in the primary member was 50 percent. The building model collapsed with a percentage of 50 at the inundation depth of 2.70 meters and indeed collapsed at the inundation depth of 4.20 meters.

(3) The comparisons between analytical and empirical fragility curves have also been discussed. Both models estimated the damage probability for residential buildings at damage level 1 obviously occurred at an inundation depth of 0.5 m. For damage level 2, the damage ratio for both models can be seen at inundation depth greater than 1.5 m, which emphasizes the vulnerability of these low-rise structures along the coastline. It is interesting to note that the damage probabilities for damage level 3 from the analytical model are higher than that of the empirical function (Inundation depth = 2 m), which might be due to the number of uncertainty variables and collapse criteria in the analysis model.

Data Availability

The data used to support the study are available from the corresponding author upon request.

Conflicts of Interest

The authors declare that they have no conflicts of interest.

References

[1] P. C. Athukorala and B. P. Resosudarmo, "The Indian Ocean tsunami: economic impact, disaster management, and lessons," *Asian Economic Papers*, vol. 4, no. 1, pp. 1–39, 2005.

[2] Usgs, *Magnitude 9.1 - off the WEST COAST of NORTHERN SUMATRA [Internet]*, United States Geological Survey, Reston, VA, USA, 2004.

[3] H. Gokon, S. Koshimura, K. Imai, M. Matsuoka, Y. Namegaya, and Y. Nishimura, "Developing fragility functions for the areas affected by the 2009 Samoa earthquake and tsunami," *Natural Hazards and Earth System Sciences*, vol. 14, no. 12, pp. 3231–3241, 2014.

[4] "National geophysical data center/world data service," *Global Historical Tsunami Database*, National Geophysical Data Center, Boulder, Colorado, 2017.

[5] National Police Agency of Japan, *Police Countermeasures and Damage Situation Associated with 2011Tohoku District - off the Pacific Ocean Earthquake*, National Police Agency of Japan, Tokyo, Japan, 2021.

[6] P. Foytong and A. Ruangrassamee, "Tsunami risk assessment of the 2004 Indian Ocean tsunami in Kamala beach Phuket," *KKU Engineering Journal*, vol. 43, no. S3, pp. 431–425, 2016.

[7] S. Koshimura, T. Oie, H. Yanagisawa, and F. Imamura, "Developing fragility functions for tsunami damage estimation using numerical model and post-tsunami data from banda aceh, Indonesia," *Coastal Engineering Journal*, vol. 51, no. 3, pp. 243–273, 2009.

[8] A. Suppasri, S. Koshimura, and F. Imamura, "Developing tsunami fragility curves based on the satellite remote sensing and the numerical modeling of the 2004 Indian Ocean tsunami in Thailand," *Natural Hazards and Earth System Sciences*, vol. 11, no. 1, pp. 173–189, 2011.

[9] A. Suppasri, E. Mas, I. Charvet et al., "Building damage characteristics based on surveyed data and fragility curves of the 2011 Great East Japan tsunami," *Natural Hazards*, vol. 66, no. 2, pp. 319–341, 2013.

[10] K. I. U. Nanayakkara and W. P. S. Dias, "Fragility curves for structures under tsunami loading," *Natural Hazards*, vol. 80, no. 1, pp. 471–486, 2016.

[11] P. Foytong and A. Ruangrassamee, "Fragility curves of reinforced-concrete buildings damaged by the 2004 tsunami," *KKU Engineering Journal*, vol. 43, no. S3, pp. 419–423, 2016.
[12] R. Aránguiz, L. Urra, R. Okuwaki, and Y. Yagi, "Development and application of a tsunami fragility curve of the 2015 tsunami in Coquimbo, Chile," *Natural Hazards and Earth System Sciences*, vol. 18, no. 8, pp. 2143–2160, 2018.
[13] Asce/Sei 41-17, *Seismic Evaluation and Retrofit of Existing Buildings*, American Society of Civil Engineers, Reston, VA, USA, 2014.
[14] A. Janpila, P. Foytong, S. T. N. Thanasisathit, and A. Ruangrassamee, "The optimal method for building damage fragility curve development," *International Journal of GEOMATE*, vol. 18, no. 69, pp. 74–80, 2020.
[15] N. Leelawat, A. Suppasri, O. Murao, and F. Imamura, "A study on the influential factors on building damage in Sri Lanka during the 2004 Indian Ocean tsunami," *Journal of Earthquake and Tsunami*, vol. 10, no. 02, Article ID 1640001, 2016.
[16] A. Suppasri, S. Koshimura, F. Imamura, A. Ruangrassamee, and P. Foytong, "A review of tsunami damage assessment methods and building performance in Thailand," *Journal of Earthquake and Tsunami*, vol. 7, no. 5, Article ID 1350036, 2013.
[17] A. Suppasri, P. Latcharote, J. D. Bricker et al., "Improvement of tsunami countermeasures based on lessons from the 2011 great east Japan earthquake and tsunami -Situation after five years-," *Coastal Engineering Journal*, vol. 58, no. 4, pp. 1640011–1640030, 2016.
[18] A. Suppasri, I. Charvet, K. Imai, and F. Imamura, "Fragility curves based on data from the 2011 tohoku-oki tsunami in Ishinomaki city, with discussion of parameters influencing building damage," *Earthquake Spectra*, vol. 31, no. 2, pp. 841–868, 2015.
[19] P. Latcharote, A. Suppasri, A. Yamashita et al., "Possible failure mechanism of buildings overturned during the 2011 great east Japan tsunami in the town of Onagawa, frontiers in built environment," earthquake engineering, mega quakes," *Cascading Earthquake Hazards and Compounding Risks*, vol. 3, no. 16, pp. 1–18, 2017.
[20] P. Foytong, A. Ruangrassamee, P. Lukkunaprasit, and N. Thanasisathit, "Behaviours of reinforced-concrete building under tsunami loading," *The IES Journal Part A: Civil & Structural Engineering*, vol. 8, no. 2, pp. 101–110, 2015.
[21] Fema 55, *Coastal Construction Manual Edition 3*, Foreign Exchange Management Act, Washington, DC, USA, 2000.
[22] H. Yeh, "Maximum fluid forces in the tsunami runup zone," *Journal of Waterway, Port, Coastal, and Ocean Engineering*, vol. 132, no. 6, pp. 496–500, 2006.
[23] H. Yeh, "Design tsunami forces for onshore structures," *Journal of Disaster Research*, vol. 2, no. 6, pp. 531–536, 2007.
[24] Fema P646, *Guidelines for Design of Structures for Vertical Evacuation from Tsunamis*, Foreign Exchange Management Act, Washington, DC, USA, 2008.
[25] P. Lukkunaprasi, N. Thanasisathit, and H. Yeh, "Experimental verification of FEMA P646 tsunami loading," *Journal of Disaster Research*, vol. 4, pp. 45–53, 2009.
[26] T. Paulay and M. J. N. Priestly, *Seismic Design of Reinforced Concrete and Masonry Buildings*, John Wiley & Sons, New York, NY, USA, 1992.
[27] H. Sezen, *Seismic behavior and modeling of reinforced concrete building columns*, Ph.D. thesis, University of California at Berkeley, Berkeley, CA, USA, 2002.
[28] H. Mostafaei and T. Kabeyasawa, "Effect of infill masonry walls on the seismic response of reinforced concrete buildings subjected to the 2003 bam earthquake strong motion," *A Case Study of Bam Telephone Center*, vol. 79, pp. 133–156, 2004.
[29] Astm C 1314-03b, *Standard Test Method for Compressive Strength of Masonry Prisms*, ASTM International, Pennsylvania, USA, 2014.
[30] P. Foytong, M. Boonpichetvong, N. Areemit, and J. Teerawong, "Effect of brick types on compressive strength of masonry prisms," *International Journal of Technology*, vol. 7, no. 7, pp. 1171–1178, 2016.
[31] Fema 306, *Evaluation of Earthquake Damaged Concrete and Masonry Wall Buildings*, Foreign Exchange Management Act, Washington, DC, USA, 1998.
[32] H. M. Fritz, J. C. Borrero, C. E. Synolakis, and J. Yoo, "Indian Ocean tsunami flow velocity measurements from survivor videos," *Geophysical Research Letters*, vol. 33, no. 24, pp. 3–7, 2004.
[33] H. Matsutomi and K. Okamoto, "Inundation flow velocity of tsunami on land," *Island Arc*, vol. 19, no. 3, pp. 443–457, 2010.
[34] P. Foytong, A. Ruangrassamee, G. Shoji, Y. Hiraki, and Y. Ezura, "Analysis of tsunami flow velocities during the March 2011 tohoku, Japan, tsunami," *Earthquake Spectra*, vol. 29, no. 1_suppl, pp. S161–S181, 2013.
[35] M. Shinozuka, M. Q. Feng, H. Kim, T. Uzawa, and T. Ueda, *Statistical Analysis of Fragility Curves*, University of Southern California, Los Angeles, CA, USA, 2001.